Progress In Electromagnetics Research M, Vol. 24, 235–249, 2012

ANTENNA PATTERN RECONSTRUCTION DIRECTLY FROM NONREDUNDANT NEAR-FIELD MEASUREMENTS COLLECTED BY A CYLINDRICAL FACILITY

F. D'Agostino, F. Ferrara, C. Gennarelli*, G. Gennarelli, R. Guerriero, and M. Migliozzi

Dipartimento di Ingegneria Elettronica e Ingegneria Informatica, University of Salerno, via Ponte Don Melillo, Fisciano, Salerno 84084, Italy

Abstract—This paper is devoted to the experimental validation of two direct near-field-far-field transformations with cylindrical scanning for elongated antennas requiring a minimum number of near-field measurements. They rely on the nonredundant sampling representations of electromagnetic fields and employ two different source modellings suitable to deal with electrically long antennas. These transformations allow the accurate reconstruction of the antenna far-field pattern in any cut plane directly from the collected near-field data without interpolating them. Their effectiveness is assessed by the good agreement between the so recovered far-field patterns and those obtained by means of the classical near-field-far-field transformation with cylindrical scanning.

1. INTRODUCTION

As well-known, near-field (NF) measurements can be profitably exploited to reconstruct antenna far-field (FF) patterns by means of NF-FF transformation techniques [1–5], when FF range size limitations, transportation and mounting problems make impractical the measurement of the radiation patterns on a conventional FF range. Moreover, the NF measurements can be performed in a controlled environment, as an indoor shielded anechoic chamber, thus overcoming the drawbacks arising in FF measurements.

The NF-FF transformation with cylindrical scanning [6–14] is particularly attractive when dealing with antennas that concentrate

Received 2 May 2012, Accepted 30 May 2012, Scheduled 6 June 2012

* Corresponding author: Claudio Gennarelli (gennar@diiie.unisa.it).

the electromagnetic (EM) radiation in an angular region centred on the horizontal plane, as those employed for radio base stations. In fact, unlike the planar scannings, it allows the reconstruction of the antenna complete radiation pattern save for the angular regions nearby the spherical polar angles, although with a slight increase in the analytical and computational complexity.

A first attempt to reduce the number of needed NF data (and, as a consequence, of measurements time) with respect to the classical transformations [6, 7] has been made in [11] by applying the spatial bandlimitation properties of the EM fields radiated by finite size sources [15]. In such a case, the number of data on each ring decreases moving from the central measurement rings to the peripheral ones, and the spacing between the rings grows when the cylinder radius increases. However, such an approach still exhibits the shortcoming that the overall number of samples becomes unbounded when the height of the scanning cylinder approaches infinity.

A more significant reduction of the number of required NF measurements has been achieved in [12–14] by applying the nonredundant sampling representations of EM fields [16]. According to these representations, the EM fields radiated by finite size sources enclosed in a convex domain bounded by a rotational surface Σ and observed on a surface M having the same rotational symmetry can be very well approximated by spatially bandlimited functions, provided that a proper phase factor is singled out from the field (or voltage acquired by a nondirective probe) and proper parameterizations are adopted for describing M. It is worth noting that the number of required samples is finite also for an unbounded observation domain, independent of it, and essentially coincident with the number of degrees of freedom of the field [16]. Two different approaches have been developed in [12–14] to reconstruct the antenna far field from the nonredundant NF measurements. An approach makes use of the optimal sampling interpolation (OSI) formulas of central type [16] to efficiently recover the NF data needed to carry out the classical cylindrical NF-FF transformations [5, 6] from the collected nonredundant ones. The other approach allows to reconstruct the antenna far field in any cut plane directly from the acquired nonredundant data without interpolating them. In particular, a spherical modelling of the antenna under test (AUT) has been adopted in [12], whereas a rounded cylinder, i.e., a cylinder ended in two half spheres and a prolate ellipsoid have been considered for electrically long antennas in [13] and [14], respectively. These last two modellings allow one to further reduce the NF data number when the antenna geometry departs significantly from the spherical one, as well as to

consider measurement cylinders with radius smaller than one half the antenna maximum size with a beneficial mitigation effect on the error related to the scanning area truncation.

An experimental validation of the interpolation based approach can be found in [17], whereas the one relevant to the direct approach when adopting a spherical AUT modelling has been provided in [18], wherein it is also highlighted the interesting property to eliminate the characteristic ripple due to the discontinuity of the near field at the edges of the scanning zone.

The aim of this paper is to provide the experimental validation of the direct NF-FF transformations with cylindrical scan for electrically long antennas [13, 14]. The experimental tests have been carried out at the UNISA Antenna Characterization Lab, where an advanced cylindrical NF measurement facility supplied by MI Technologies is available. It must be stressed that, in both the cases, the sampling arrangements have been properly modified in order to have a symmetrical distribution of rings with respect to the middle plane. Moreover, the ideal probe assumption originally made in [13] has been removed.

2. SAMPLING REPRESENTATION ON A CYLINDER

Let us consider an AUT, enclosed in a convex domain bounded by a surface Σ with rotational symmetry, a nondirective probe scanning a cylinder of radius d in the NF region and adopt the spherical coordinate system (r, ϑ, φ) to denote an observation point P. Since, for such a kind of a probe, the output voltage has the same effective spatial bandwidth of the AUT field and a cylindrical surface can be represented by generatrices and rings, in the following we deal with the voltage representation on an observation curve C characterized by an analytical parameterization $\underline{r} = \underline{r}(\xi)$. According to [16], it is convenient to introduce the "reduced voltage"

$$\tilde{V}(\xi) = V(\xi)e^{\mathrm{j}\psi(\xi)}, \tag{1}$$

where $V(\xi)$ is the measured probe voltage, $\psi(\xi)$ is a proper phase function and ξ is an optimal parameter used to describe C. The bandlimitation error, occurring when $\tilde{V}(\xi)$ is approximated by a spatially bandlimited function, becomes negligible as the bandwidth exceeds a critical value W_ξ [16]. In fact, it exhibits a step-like behaviour whose transition occurs at W_ξ [15]. Therefore, such an error can be effectively controlled by choosing a bandwidth equal to $\chi' W_\xi$, where $\chi' > 1$ is the bandwidth enlargement factor.

When the observation curve is a generatrix, by adopting $W_\xi = \beta\ell'/2\pi$ (β is the wavenumber and ℓ' is the length of the curve C',

obtained as intersection between the meridian plane passing through the point P and Σ), we get:

$$\psi = \frac{\beta}{2}\left[R_1 + R_2 + s_1' - s_2'\right]; \quad \xi = \frac{\pi}{\ell'}\left[R_1 - R_2 + s_1' + s_2'\right] \tag{2}$$

wherein $s_{1,2}'$ are the arclength coordinates of the tangency points $P_{1,2}$ between the cone of vertex at P and C'.

When C is a ring, ψ is constant and then it can be chosen coincident with the value relevant to the generatrix passing through P. Moreover, it is convenient to use the azimuthal angle φ as parameter. The corresponding bandwidth is given [16] by:

$$\begin{aligned} W_\varphi &= \frac{\beta}{2}\max_{z'}(R^+ - R^-) \\ &= \frac{\beta}{2}\max_{z'}\left(\sqrt{(z-z')^2+(d+\rho'(z'))^2} - \sqrt{(z-z')^2+(d-\rho'(z'))^2}\right) \end{aligned} \tag{3}$$

wherein $\rho'(z')$ is the equation of Σ in cylindrical coordinates. By using the triangular inequality, it can be easily shown that the following bound for W_φ holds:

$$W_\varphi \leq \beta\rho_{\max} \tag{4}$$

$\rho_{\max}$ being the maximum transverse radius of Σ.

By taking into account the above results, the voltage at any point P on the generatrix at φ can be evaluated by means of the following OSI expansion:

$$\tilde{V}\left(\xi(\vartheta),\varphi\right) = \sum_{n=n_0-q+1}^{n_0+q} \tilde{V}\left(\xi_n,\varphi\right) \Omega_N\left(\xi-\xi_n\right) D_{N''}\left(\xi-\xi_n\right) \tag{5}$$

where $n_0 = \mathrm{Int}\left[(\xi - \Delta\xi/4)/\Delta\xi\right]$ is the index of the sample nearest (on the left) to P, $2q$ is the number of retained intermediate samples $\tilde{V}\left(\xi_n,\varphi\right)$, namely, the reduced voltage values at the intersection points between the rings and the considered generatrix, and

$$\xi_n = n\Delta\xi + \Delta\xi/4; \quad \Delta\xi = 2\pi/\left(2N''+1\right) \tag{6}$$

$$N'' = \mathrm{Int}(\chi\, N') + 1; \quad N' = \mathrm{Int}(\chi' W_\xi) + 1 \tag{7}$$

$\chi > 1$ is an oversampling factor [16], and $\mathrm{Int}(x)$ denotes the integer part of x. In (5),

$$\begin{aligned} D_{N''}\left(\xi\right) &= \frac{\sin\left[(2N''+1)\,\xi/2\right]}{(2N''+1)\,\sin(\xi/2)}; \\ \Omega_N\left(\xi\right) &= \frac{T_N\left[2\cos^2\left(\xi/2\right)/\cos^2\left(\bar{\xi}/2\right)-1\right]}{T_N\left[2/\cos^2\left(\bar{\xi}/2\right)-1\right]} \end{aligned} \tag{8}$$

are the Dirichlet and Tschebyscheff sampling functions [16], $T_N(\cdot)$ being the Tschebyscheff polynomial of degree $N = N'' - N'$ and $\bar{\xi} = q\Delta\xi$. Note that the shift $\Delta\xi/4$ in the sampling position allows to have a symmetrical distribution of rings with respect to $z = 0$, thus giving rise to an equal amount of truncation error at both the cylinder ends.

The intermediate samples $\tilde{V}(\xi_n, \varphi)$ can be reconstructed [13, 14] via an OSI expansion along φ, quite similar to (5) and not reported here for space saving, thus allowing to retrieve the probe voltage at any point on the scanning cylinder from a nonredundant number of its samples. It is so possible to recover the NF data needed to carry out the classical NF-FF transformation with cylindrical scanning [6] or [7].

2.1. The Prolate Ellipsoidal Modelling

An effective modelling for elongated antennas is obtained by choosing the surface Σ coincident with a prolate ellipsoid having major and minor semi-axes equal to a and b (see Fig. 1). In such a case, the bandwidth W_ξ, the optimal expressions for the phase factor ψ and parameterization ξ relevant to a cylinder generatrix become [14, 16]:

$$W_\xi = \frac{4a}{\lambda} E\left(\pi/2 \,|\varepsilon^2\right); \quad \xi = \frac{\pi}{2}\left[1 + \frac{E\left(\sin^{-1} u \,|\varepsilon^2\right)}{E\left(\pi/2 \,|\varepsilon^2\right)}\right] \tag{9}$$

$$\psi = \beta a \left[v\sqrt{\frac{v^2-1}{v^2-\varepsilon^2}} - E\left(\cos^{-1}\sqrt{\frac{1-\varepsilon^2}{v^2-\varepsilon^2}}\,|\varepsilon^2\right)\right] \tag{10}$$

where $E(\cdot|\cdot)$ denotes the elliptic integral of second kind, λ is the wavelength, and $u = (r_1 - r_2)/2f$ and $v = (r_1 + r_2)/2a$ are the elliptic coordinates, $r_{1,2}$ being the distances from the observation point P to the foci of the ellipse C'. Moreover, $\varepsilon = f/a$ is the eccentricity of C', $2f$ being its focal distance. The expression of ξ in (9) is valid when the angle ϑ belongs to the range $[0, \pi/2]$. The case in which ϑ belongs to $[\pi/2, \pi]$ can be easily handled by determining the value ξ' corresponding to the point specified by the angle $\pi - \vartheta$ and then setting $\xi = \pi - \xi'$. As shown in [16], the curves $\psi = \text{const}$ and $\xi = \text{const}$ are ellipses and hyperbolas confocal to C'. Moreover, the bandwidth W_φ is

$$W_\varphi(\xi) = \beta b \sin\vartheta_\infty(\xi) \tag{11}$$

$\vartheta_\infty = \sin^{-1} u + \pi/2$ being the polar angle of the asymptote to the hyperbola through P.

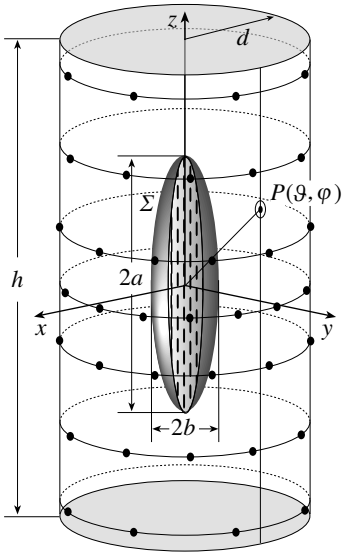

Figure 1. Cylindrical scanning: prolate ellipsoidal modelling.

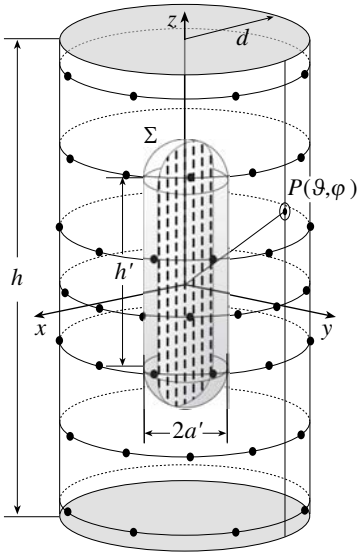

Figure 2. Cylindrical scanning: rounded cylinder modelling.

2.2. The Rounded Cylinder Modelling

An alternative effective modelling for elongated antennas is obtained by considering them as enclosed in a cylinder of height h' ended in two half-spheres of radius a' (see Figs. 2 and 3). In such a case, the bandwidth W_ξ can be obtained by taking into account that $\ell' = 2(h' + \pi a')$, whereas the optimal expressions for the phase factor ψ and parameterization ξ relevant to a generatrix can be determined by substituting in (2) the appropriate values of $s'_{1,2}$ and $R_{1,2}$, whose expressions, as shown in [13], are:

$$R_{1,2} = \sqrt{(z \mp h'/2)^2 + d^2 - a'^2}; \quad s'_1 = a' \sin^{-1}\left(\frac{a'd + R_1\left((h'/2) - z\right)}{R_1^2 + a'^2}\right) \tag{12}$$

$$s'_2 = h' + a' \left[\pi - \sin^{-1}\left(\frac{a'd + R_2\left((h'/2) + z\right)}{R_2^2 + a'^2}\right)\right] \tag{13}$$

As regards W_φ, it can be shown [13] that the maximum in (3) is attained at

$$z' = \begin{cases} z & |z| \le h'/2 \\ \left[\dfrac{h'}{2} + \dfrac{(|z| - h'/2)\, a'^2}{d^2 + (|z| - h'/2)^2}\right] \mathrm{sgn}(z) & |z| > h'/2 \end{cases} \tag{14}$$

where sgn $(\cdot)$ is the sign function.

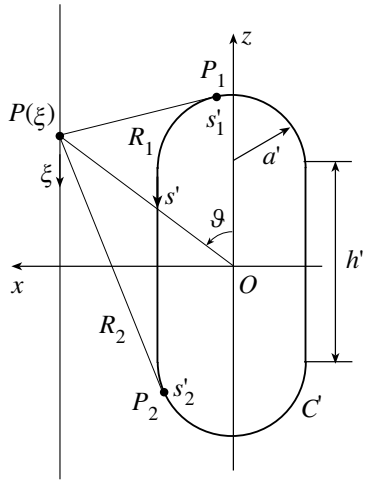

Figure 3. Rounded cylinder modelling: relevant to a cylinder generatrix.

3. CLASSICAL NF-FF TRANSFORMATION

According to the classical probe compensated NF-FF transformation with cylindrical scanning [6], the cylindrical wave expansion coefficients a_ν and b_ν of the AUT field are related to: i) the two-dimensional Fourier transforms $I_\nu^{1,2}$ of the voltage acquired by the probe in two independent sets of measurements (the probe is rotated 90° about its longitudinal axis in the second set); ii) the cylindrical wave expansion coefficients (c_m, d_m) and $(c'_m,\ d'_m)$ of the field radiated by the probe and the rotated probe, when used as transmitting antennas. As shown in [6], it results:

$$a_\nu(\eta) = \frac{\beta^2}{\Lambda^2 \Delta_\nu(\eta)} \left[I_\nu^1(\eta) \sum_{m=-\infty}^{\infty} d'_m(-\eta) H_{\nu+m}^{(2)}(\Lambda d) - I_\nu^2(\eta) \sum_{m=-\infty}^{\infty} d_m(-\eta) H_{\nu+m}^{(2)}(\Lambda d) \right] \tag{15}$$

$$b_\nu(\eta) = \frac{\beta^2}{\Lambda^2 \Delta_\nu(\eta)} \left[I_\nu^2(\eta) \sum_{m=-\infty}^{\infty} c_m(-\eta) H_{\nu+m}^{(2)}(\Lambda d) - I_\nu^1(\eta) \sum_{m=-\infty}^{\infty} c'_m(-\eta) H_{\nu+m}^{(2)}(\Lambda d) \right] \tag{16}$$

$$\Delta_\nu(\eta) = \sum_{m=-\infty}^{\infty} c_m(-\eta)\, H^{(2)}_{\nu+m}(\Lambda d) \sum_{m=-\infty}^{\infty} d'_m(-\eta)\, H^{(2)}_{\nu+m}(\Lambda d) - \sum_{m=-\infty}^{\infty} c'_m(-\eta)\, H^{(2)}_{\nu+m}(\Lambda d) \sum_{m=-\infty}^{\infty} d_m(-\eta)\, H^{(2)}_{\nu+m}(\Lambda d) \quad (17)$$

$$I^{1,2}_\nu(\eta) = \int_{-\infty}^{\infty}\int_{-\pi}^{\pi} V^{1,2}(\varphi, z)\; e^{-j\nu\varphi}\, e^{j\eta z}\, d\varphi\, dz \quad (18)$$

where $\Lambda = (\beta^2 - \eta^2)^{1/2}$, $H^{(2)}_\nu(\cdot)$ is the Hankel function of second kind and order ν, and V^1, V^2 are the output voltages of the probe and the rotated probe at the point of cylindrical coordinates (d, φ, z).

In the classical approach [6], the fast Fourier transform (FFT) is employed to evaluate in an efficient way the Fourier transforms (18) of the probe and rotated probe voltages, and the NF data are collected on a cylindrical grid wherein the sample spacing Δz between the rings is smaller than one half a wavelength and the one $\Delta\varphi$ on each of them is fixed according to the so called minimum cylinder law, i.e.,

$$\Delta z \;\le\; \lambda/2; \quad \Delta\varphi \;\le\; \pi/(\beta\rho') \;=\; \lambda/(2\rho') \quad (19)$$

ρ' being the radius of the smallest cylinder enclosing the AUT. In practice, $\Delta\varphi$ is chosen such that the number of samples N_c on each ring is the smallest integer, power of two or product of powers of 2, 3 and 5, equal or greater than $2[\mathrm{Int}(\beta\rho') + 10]$, depending on the available routine implementing the FFT algorithm. It must be stressed that the rigorous justification of the minimum cylinder law is a trivial consequence of (4).

At last, the FF spherical components of the electric field are determined by means of the following relations:

$$E_\vartheta(r, \vartheta, \varphi) = F_\vartheta(\vartheta, \varphi)\, \frac{e^{-\mathrm{j}\beta r}}{r} = -\mathrm{j}2\beta \frac{e^{-\mathrm{j}\beta r}}{r} \sin\vartheta \sum_{\nu=-\infty}^{\infty} \mathrm{j}^\nu b_\nu(\beta\cos\vartheta)\, e^{\mathrm{j}\nu\varphi} \quad (20)$$

$$E_\varphi(r, \vartheta, \varphi) = F_\varphi(\vartheta, \varphi)\, \frac{e^{-\mathrm{j}\beta r}}{r} = -2\beta \frac{e^{-\mathrm{j}\beta r}}{r} \sin\vartheta \sum_{\nu=-\infty}^{\infty} \mathrm{j}^\nu a_\nu(\beta\cos\vartheta)\, e^{\mathrm{j}\nu\varphi} \quad (21)$$

which can be efficiently evaluated via the FFT algorithm.

4. DIRECT NF-FF TRANSFORMATION

By taking into account (5), we can rewrite the Fourier transforms (18) in the form:

$$I_\nu^{1,2}(\eta) = \sum_{n\in N_r} \int_{-\infty}^{\infty} \int_{-\pi}^{\pi} \tilde{V}^{1,2}(\xi_n,\varphi)\ D_{N''}(\xi(z)-\xi_n) \cdot Q(\xi(z)-\xi_n)\ e^{-j\psi(z)} e^{-j\nu\varphi} e^{j\eta z} d\varphi\, dz \tag{22}$$

N_r being the indexes set of all considered NF rings and $Q = \Omega_N$, if $|\xi(z)-\xi_n| \le q\Delta\xi$, or $Q = 0$, otherwise. It is convenient to express $\tilde{V}^{1,2}$ as a Fourier series in φ, namely,

$$\tilde{V}^{1,2}(\xi_n,\varphi) = \sum_{k=-M'}^{M'} \tilde{V}_k^{1,2}(\xi_n)\ e^{jk\varphi} \tag{23}$$

where M' is the smallest integer, obtained as product of the prime factors 2, 3, and 5, greater or equal to $\mathrm{Int}[\chi^* W_\varphi(\xi_n)] + 1$ and $\chi^* = 1 + (\chi' - 1)[\sin\vartheta(\xi_n)]^{-2/3}$. By substituting (23) in (22), it results:

$$I_\nu^{1,2}(\eta) = \sum_{n\in N_r} \tilde{V}_\nu^{1,2}(\xi_n)\, G_{n\eta} \tag{24}$$

wherein

$$G_{n\eta} = 2\pi \int_{z_i}^{z_f} D_{N''}(\xi(z) - \xi_n)\, \Omega_N(\xi(z) - \xi_n)\, e^{-j\psi(z)} e^{j\eta z} dz \tag{25}$$

with $z_i = z(\xi_n + q\Delta\xi)$ and $z_f = z(\xi_n - q\Delta\xi)$.

As shown in [18], the direct NF-FF transformation exhibits the very interesting feature to eliminate the ripple due to the discontinuity of the near field at the scanning zone edges. This is due to the different method adopted to compute $I_\nu^{1,2}$. In fact, in the classical transformations [6, 7], they are evaluated via FFT by taking into account only the NF data falling in the scanning zone and, therefore, the integration over z is truncated to the measurement cylinder height. Whereas, in the direct NF-FF transformation, according to (25), the effect of each NF sample is considered in the range $[z_i, z_f]$, so that the peripheral samples affect the evaluation even far from the scanning area. Thus, this technique intrinsically eliminates the field discontinuity at the scanning zone edges.

It is worth noting that the $G_{n\eta}$ values can be evaluated (once and for all) for given sets of antennas, since they depend only on the

measurement cylinder radius and on the geometric parameters of the AUT modelling.

By summing up, the far field can be evaluated through the following steps: i) the samples of V^1 and V^2 are multiplied by the phase factor $e^{j\psi}$ and the corresponding Fourier series coefficients are calculated via FFT; ii) for each required value of ϑ, fixing the corresponding value of η by the relation $\eta = \beta\cos\vartheta$, the $G_{n\eta}$ values are computed or read, if pre-calculated. Then, the Fourier transforms $I_\nu^{1,2}(\eta)$ are determined by performing the summations (24). The corresponding values of the modal coefficients a_ν and b_ν can be finally obtained. Once they have been calculated, the FF spherical components of the electric field are determined by evaluating (20) and (21) via the FFT.

From the efficiency viewpoint, it is convenient to use this method to evaluate only the FF samples necessary to recover the antenna pattern via the following far-field OSI expansion using even numbers of samples along the meridians and parallels [13, 14]:

$$F_{\vartheta,\varphi}(\vartheta(\xi),\varphi) = \frac{2N_F''-1}{2N_F''} \sum_{n=n_0-q+1}^{n_0+q} \left\{ \Omega_{N_F}(\xi-\xi_n) D_{N_F''-1}(\xi-\xi_n) \frac{2M_n''-1}{2M_n''} \right.$$

$$\left. \cdot \sum_{m=m_0-p+1}^{m_0+p} F_{\vartheta,\varphi}(\xi_n,\varphi_{m,n}) \Omega_{M_n}(\varphi-\varphi_{m,n}) D_{M_n''-1}(\varphi-\varphi_{m,n}) \right\} \tag{26}$$

wherein $n_0 = \mathrm{Int}\,[\xi/\Delta\xi]$ and $m_0 = \mathrm{Int}\,[\varphi/\Delta\varphi_n]$ are the indexes of the sample nearest (on the left) to the output point, and

$$\xi_n = n\Delta\xi = n\pi/N_F''; \quad N_F'' = 2\big[\mathrm{Int}(\chi\, N'/2)+1\big]; \quad N_F = N_F''-N' \tag{27}$$

$$\varphi_{m,n} = m\Delta\varphi_n = m\pi/M_n''; \quad M_n'' = 2^i \geq \mathrm{Int}(\chi M_n') + 1;$$

$$M_n' = \mathrm{Int}[\chi^* W_\varphi(\xi_n)] + 1 \tag{28}$$

$$M_n = M_n'' - M_n' \tag{29}$$

Obviously, there is no need to extract the phase factor $e^{-\mathrm{j}\psi(\xi)}$ from the FF expression, since it is constant on the FF sphere. The need of an OSI expansion using an even number of samples along the parallels is due to the employment of an efficient power of two FFT algorithm for computing (20) and (21). Whereas, N_F'' has been chosen according to (27) in order to have FF samples on the equator.

It is worth noting that, when adopting the rounded cylinder modelling, the expressions of W_φ and ξ relevant to the FF representation are simpler than those valid in the NF region. In fact, as shown in [13], they become:

$$W_\varphi = W_\varphi\,(\vartheta(\xi)) = \beta a' \sin\,(\vartheta(\xi))\,; \quad \xi = \frac{\pi}{\ell'}\,\left[(1-\cos\vartheta)\,h' + 2a'\vartheta\right] \tag{30}$$

At last, it must be pointed out that the direct NF-FF transformation allows the accurate reconstruction of the antenna far field in any cut plane at $\varphi =$ constant and not only in those attainable by computing (20) and (21) via the FFT algorithm.

5. EXPERIMENTAL RESULTS

The experimental validation of the described direct cylindrical NF-FF transformations has been performed in the anechoic chamber of the UNISA Antenna Characterization Lab. An open-ended WR90 rectangular waveguide is used as probe and its response has been collected on a cylinder with $d = 19.6\,\text{cm}$ and $h = 240\,\text{cm}$. The amplitude and phase measurements are carried out by means of a vectorial network analyzer. Two antennas have been employed in the experimental tests, both working at 10 GHz.

The first AUT is a H-plane monopulse antenna, located in the plane $y = 0$ and operating in the sum mode. It has been realized by using two pyramidal horns ($8.9 \times 6.8\,\text{cm}$) at a distance of 26 cm (between centers) and a hybrid tee (for its photo see [19]). It has been modelled as enclosed in a prolate ellipsoid with $a = 24\,\text{cm}$ and $b = 6\,\text{cm}$.

The direct NF-FF transformation incorporates the probe characterization, therefore, we have first of all characterized (see the Appendix of [18]) the employed probe according to [20], as done in the software package MI-3000 implementing the standard probe compensated NF-FF transformation [7], and verified that practically identical results are obtained when the same NF data are transformed by using the MI package and our so developed version of the probe compensated NF-FF transformation [6].

In Figs. 4 and 5, the H-plane and E-plane FF patterns reconstructed by using the direct NF-FF transformation based on the ellipsoidal AUT modelling are compared with those obtained via the MI software (reference pattern 1). As can be seen, the H-plane patterns are practically indistinguishable, whereas very small differences are present in the E-plane in the zones characterized by low field levels. They are due to the fact that two different NF data sets have been used. This can be overcome by retrieving, via a proper interpolation expansion, the NF data needed by the software package MI-3000 from the same data used by the nonredundant direct NF-FF transformation. A better agreement thus results comparing the reconstructed E-plane with this new FF pattern (reference pattern 2).

The second AUT is an E-plane monopulse antenna, again located in the plane $y = 0$ and operating in the sum mode. It has

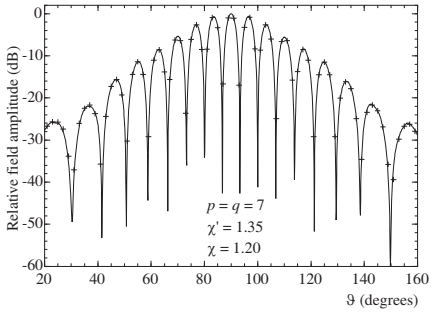

Figure 4. *H*-plane pattern. Solid line: reference pattern 1. Crosses: reconstructed via the direct NF-FF transformation using the prolate ellipsoidal modelling.

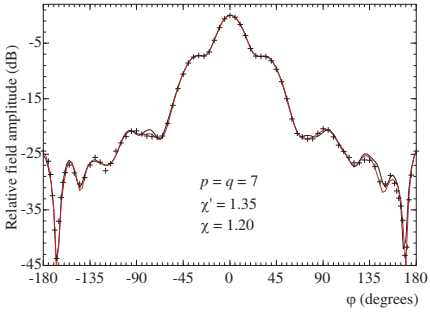

Figure 5. *E*-plane pattern. Black solid line: reference pattern 1. Red solid line: reference pattern 2. Crosses: reconstructed via the direct NF-FF transformation using the prolate ellipsoidal modelling.

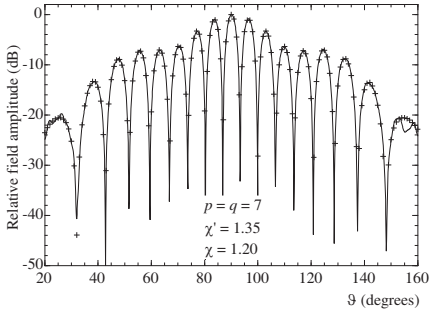

Figure 6. *E*-plane pattern. Solid line: reference pattern 1. Crosses: reconstructed via the direct NF-FF transformation using the rounded cylinder modelling.

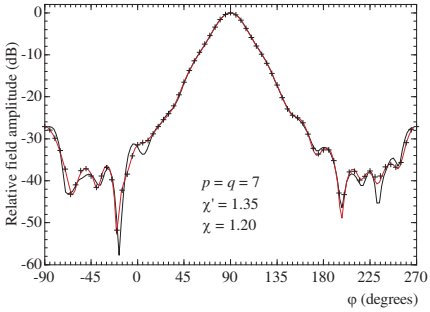

Figure 7. *H*-plane pattern. Black solid line: reference pattern 1. Red solid line: reference pattern 2. Crosses: reconstructed via the direct NF-FF transformation using the rounded cylinder modelling.

been assembled by using the same horns, whose centers in this case are distant 26.5 cm, and a hybrid tee. A rounded cylinder with $h' = 33.3$ cm and $a' = 4.95$ cm has been now adopted to model it. Fig. 6 shows the reconstruction in *E*-plane, whereas Fig. 7 shows the comparison between the reconstructed *H*-plane pattern and those obtained from the directly acquired classical cylindrical data using the MI software (reference pattern 1) and from the data retrieved via

interpolation from the nonredundant ones (reference pattern 2). The same comments as for Figs. 4 and 5 hold. The results in Fig. 6 confirm the peculiar characteristics of the developed technique to eliminate the ripple caused by the discontinuity of the near field at the edges of the scanning surface. This effect is now visible, since the near field level at the edge of the scanning cylinder is about 20 dB higher than in the first example.

It is interesting to compare the numbers of NF data used by the direct NF-FF transformation based on the prolate ellipsoidal modelling (1638) when considering the former AUT and on the rounded cylinder one (1422) for the latter, with that (5796) required by the MI software to perform the transformation for both the antennas.

For what concerns the time needed for the NF data acquisition, the proposed technique is certainly quicker than the traditional one, since the number of measurement rings is lower than the one relevant to the classical technique. Accordingly, by assuming for both the techniques the same time to acquire the NF data on each ring[†], the measurement times are directly proportional to the numbers of needed rings. For what concerns the comparison between the different NF-FF transformation techniques from the computational viewpoint, it can be found in [12] and stays valid also for the direct transformations in [13] and [14].

6. CONCLUSION

Two direct nonredundant NF-FF transformations with cylindrical scanning for electrically long antennas have been experimentally validated in this paper. They make use of a minimum number of NF data and are based on two different source modellings (the prolate ellipsoidal and the rounded cylinder one) particularly suitable to deal with electrically long antennas, but at the same time quite general. These transformations allow one to accurately reconstruct the antenna FF pattern in any cut plane directly from the acquired NF data without interpolating them and exhibit the interesting property to eliminate the characteristic ripple due to the discontinuity of the near field at the edges of the scanning zone. The experimental results, carried out at the UNISA Antenna Characterization Lab, have proved the effectiveness and the accuracy of both these techniques. Accordingly, since there is no practical difference between them from a computational viewpoint, the choice depends only on the modelling which better fits the actual AUT geometry.

[†] The number of NF data on each ring can be significantly lower for the proposed technique on the peripheral ones.

REFERENCES

1. Appel-Hansen, J., J. D. Dyson, E. S. Gillespie, and T. G. Hickman, "Antenna measurements," *The Handbook of Antenna Design*, A. W. Rudge, K. Milne, A. D. Olver, and P. Knight, Eds., Chapter 8, Peter Peregrinus Ltd., London, UK, 1982.
2. Yaghjian, A. D., "An overview of near-field antenna measurements," *IEEE Trans. Antennas Propagat.*, Vol. 34, 30–45, Jan. 1986.
3. Gillespie, E. S., "Special Issue on near-field scanning techniques," *IEEE Trans. Antennas Propagat.*, Vol. 36, 727–901, Jun. 1988.
4. Gennarelli, C., G. Riccio, F. D'Agostino, and F. Ferrara, *Near-field-far-field Transformation Techniques*, Vol. 1, CUES, Salerno, Italy, 2004.
5. Francis, M. H. and R. W. Wittmann, "Near-field scanning measurements: Theory and practice," *Modern Antenna Handbook*, C. A. Balanis, Ed., Chapter 19, John Wiley & Sons, Inc., Hoboken, NJ, USA, 2008.
6. Leach, Jr., W. M. and D. T. Paris, "Probe compensated near-field measurements on a cylinder," *IEEE Trans. Antennas Propagat.,* Vol. 21, 435–445, Jul. 1973.
7. Yaghjian, A. D., "Near-field antenna measurement on a cylindrical surface: A source scattering matrix formulation," NBS Tech. Note 696, U.S. Government Printing Office, Washington, DC, Sep. 1977.
8. Joy, E. B., W. M. Leach, Jr., G. P. Rodrigue, and D. T. Paris, "Applications of probe-compensated near-field measurements," *IEEE Trans. Antennas Propagat.*, Vol. 26, 379–389, May 1978.
9. Borgiotti, G. V., "Integral equation formulation for probe corrected far-field reconstruction from measurements on a cylinder," *IEEE Trans. Antennas Propagat.*, Vol. 26, 572–578, Jul. 1978.
10. Appel-Hansen, J., "On cylindrical near-field scanning techniques," *IEEE Trans. Antennas Propagat.*, Vol. 28, 231–234, Mar. 1980.
11. Bucci, O. M. and C. Gennarelli, "Use of sampling expansions in near-field-far-field transformations: The cylindrical case," *IEEE Trans. Antennas Propagat.*, Vol. 36, 830–835, Jun. 1988.
12. Bucci, O. M., C. Gennarelli, G. Riccio, and C. Savarese, "Non redundant representation of the electromagnetic fields over a cylinder with application to the near-field-far-field transformation," *Electromagnetics*, Vol. 16, 273–290, May 1996.

13. Bucci, O. M., C. Gennarelli, G. Riccio, and C. Savarese, "NF-FF transformation with cylindrical scanning: An effective technique for elongated antennas," *IEE Proc. — Microw., Antennas and Propagat.*, Vol. 145, 369–374, Oct. 1998.
14. D'Agostino, F., F. Ferrara, C. Gennarelli, G. Riccio, and C. Savarese, "NF-FF transformation with cylindrical scanning from a minimum number of data," *Microw. Opt. Technol. Lett.*, Vol. 35, 264–270, Nov. 2002.
15. Bucci, O. M. and G. Franceschetti, "On the spatial bandwidth of scattered fields," *IEEE Trans. Antennas Propagat.*, Vol. 35, 1445–1455, Dec. 1987.
16. Bucci, O. M., C. Gennarelli, and C. Savarese, "Representation of electromagnetic fields over arbitrary surfaces by a finite and nonredundant number of samples," *IEEE Trans. Antennas Propagat.*, Vol. 46, 351–359, Mar. 1998.
17. Bucci, O. M. and C. Gennarelli, "Application of nonredundant sampling representations of electromagnetic fields to NF-FF transformation techniques," *Int. Jour. of Antennas and Propagat.*, Vol. 2012, Article ID 319856, 14 pages, 2012.
18. D'Agostino, F., F. Ferrara, C. Gennarelli, R. Guerriero, and M. Migliozzi, "On the direct nonredundant near-field-far-field transformation in a cylindrical scanning geometry," *IEEE Antennas Propagat. Magazine*, Vol. 54, 130–138, Feb. 2012.
19. D'Agostino, F., F. Ferrara, C. Gennarelli, R. Guerriero, and M. Migliozzi, "Laboratory tests assessing the effectiveness of the NF-FF transformation with helicoidal scanning for electrically long antennas," *Progress In Electromagnetics Research*, Vol. 98, 375–388, 2009.
20. Yaghjian, A. D., "Approximate formulas for the far field and gain of open-ended rectangular waveguide," *IEEE Trans. Antennas Propagat.*, Vol. 34, 378–384, Apr. 1984.